Nanoscale Advances

ROYAL SOCIETY OF CHEMISTRY

PAPER

View Article Online
View Journal | View Issue

Cite this: *Nanoscale Adv.*, 2025, **7**, 2751

Renal clearable sucrose carbon dots for doxorubicin delivery to treat renal carcinoma†

Farhana Azmi, ‡[ab] Xiaoxue Xu, ‡[c] Hien Duong,[b] Ping Ye,[a] Titi Chen,[ab] Hongxi Li,[a] Jianwei Chen,[ab] Sara Madadi Ardekani,[a] Alireza Dehghani,[a] Guoping Zheng,[ab] David Harris,[ab] Hongxu Lu,[c] Yiping Wang‡[ab] and Qi Cao‡[ab]

Received 30th December 2024
Accepted 18th March 2025

DOI: 10.1039/d4na01082e

rsc.li/nanoscale-advances

Renal Cell Carcinoma (RCC) poses challenges for conventional treatment methods, but recent advancements indicate the potential of nanoparticles (NPs) in enhancing chemotherapy efficacy. This study focuses on developing non-toxic NPs from sucrose and L-serine *via* hydrothermal synthesis to produce Sucrose Carbon Dots (Suc CDs), designed for renal clearance to deliver hydrophilic drugs for the treatment of RCC. Suc CDs with a size of 4 nm exhibit high fluorescence with a fluorescence quantum yield of 58% and high drug loading capacity without toxicity to normal cell lines (renal tubular cells). Under *in vitro* conditions, Suc CDs alone are non-toxic, while Suc CDs with DOX display improved anticancer effects on Renca cells (cancer cell line). Under *in vivo* conditions, Suc CDs loaded with DOX outperform DOX alone with reduced toxicity to normal cells. Biodistribution study of Suc CDs revealed prolonged tumour site accumulation. This research demonstrates that renal clearable Suc CDs loaded with DOX exhibit superior anti-cancer activity, and are free of side effects, suggesting promising therapeutic potential for human RCC.

Introduction

Kidney cancer is a disease with increasing global incidence, estimated at 400 000 new cases annually, and a worldwide mortality rate nearing 175 000 deaths per year.[1] Renal cell carcinoma (RCC), particularly the clear cell subtype, constitutes about 75% of cases and is notably aggressive, being the leading cause of kidney cancer-related deaths.[2,3] Despite curative interventions for localized RCC, approximately 30% of clear cell RCC patients eventually develop metastasis, often leading to fatal outcomes.[4] Among urologic tumours, RCC has the highest cancer specific mortality rate and RCC incidence increases markedly with age.[5] Distant metastases primarily occur in the lungs, lymph nodes, liver, bone, and brain.[6] RCC lacks early symptoms, resists radiation and chemotherapy, with limited responses to immunotherapeutic agents.[7] Despite recent treatment advancements, durable complete remissions are rare, and advanced RCC remains a lethal disease.[8] The key challenge in treatment lies in precise targeting of therapeutic agents to ensure effective cancer cell destruction while minimizing off-target drug delivery to healthy cells.[9]

Nanomedicine, bridging biology, medicine, engineering, and chemistry, holds great promise in advancing cancer diagnosis and treatment. Recent breakthroughs involve nanocarriers (10 nm to 100 nm) for cancer therapeutics, including FDA-approved nanocarrier liposomes and albumin nanoparticles like Doxil.[9] Nanoparticles (NPs) as a drug carrier have several advantages over traditional chemotherapy for cancer treatments, including (a) improved solubility of hydrophobic drugs; (b) protection of the compound from undesirable interaction with external stimuli and improved stability; (c) a controlled drug release profile and longer circulation time; and (d) an enhanced permeability and retention effect in specific tissues or organs by passive targeting and specific ligand conjugation induced by active targeting.[10]

Carbon material-based nanoparticles, such as Carbon Dots (CDs), carbon nanotubes (CNTs), and Graphene Quantum Dots (GQDs), have gained attention as drug carriers because of their extremely small size, excellent biocompatibility, easy surface modifications and high drug loading efficiency.[11] Modulating particle characteristics enables localization to specific body sites, with renal clearance being a desirable property for eliminating potentially toxic nanomaterials.[12] Renal clearable nanoparticles with tuneable size, shape, and surface chemistry can avoid major organ accumulation.[13] Doxorubicin is a commonly used chemotherapeutic agent for many solid tumours, but this has many disadvantages, which includes low permeability and retention, low cell internalization, and cytotoxicity to healthy cells. These can be

[a]*Centre for Transplantation and Renal Research, Westmead Institute for Medical Research, The University of Sydney, NSW, Australia. E-mail: fazm3421@uni.sydney.edu.au; farah.s.azmi@gmail.com; qi.cao@sydney.edu.au*

[b]*Faculty of Medicine and Health, The University of Sydney, NSW, Australia*

[c]*Institute for Biomedical Materials and Devices, University of Technology Sydney, Australia*

† Electronic supplementary information (ESI) available. See DOI: https://doi.org/10.1039/d4na01082e

‡ These authors contributed equally.

overcome by using nanocarriers for targeted tumour delivery with increased permeability and retention on the cancer cells.[14]

Renal clearance of intravascular agents by the kidneys is a process involving glomerular filtration, tubular secretion, and removal of the molecule *via* urine excretion. Glomerular filtration is dependent on the particle size which is known as the filtration size threshold. Molecules with a hydrodynamic diameter of <6 nm are filtered through the glomerulus, while particles >8 nm are not typically capable of undergoing glomerular filtration. Renal clearance studies in mice demonstrated that quantum dots with a size ranging from 4.36 to 5.52 nm were excreted *via* the kidneys but quantum dots with a size more than 8 nm were up taken by the reticuloendothelial system (RES) and lung.[15] NPs with a size larger than 10 nm have increased long term toxicity concerns due to their fast and high uptake by the reticuloendothelial system.[16]

The approach for nanomedicine development includes specific targeting, real-time imaging, and minimal side effects. Targeted therapy has improved renal cell carcinoma outcomes, with nanoparticle-conjugated drugs in clinical trials. The emergence of renal clearable NPs addresses long-term challenges, offering potential as renal nanomedicine for treating renal cell carcinoma. This study focuses on novel renal clearable carbon dot nanoparticles, hypothesizing their efficacy in delivering doxorubicin for renal cell carcinoma treatment, demonstrated at the cellular level in mice models. In this study, we synthesized carbon dots from sucrose and L-serine *via* the hydrothermal method. The prepared CDs and Dox form a complex by non-covalent bonding *via* electrostatic interactions or by hydrogen bonds between the carboxylic group on CDs and the amine moiety on DOX.[17,18] One of the key challenges in drug delivery systems is ensuring a sustained drug release profile and prolonged circulation time. It was discovered that drug loading is feasible at neutral pH, primarily driven by electrostatic interactions. The presence of additional hydrogen bonds in the drug–carrier complex enhances loading efficiency, while drug release remains pH-dependent. The pH-sensitive release mechanism within the tumour microenvironment is another factor that can elevate the local concentration of chemotherapeutic agents, thereby improving therapeutic efficacy under acidic conditions characteristic of the tumour microenvironment.[19,20] The physicochemical properties of the Suc CDs were investigated by using transmission electron microscopy (TEM), X-ray diffraction analysis, Fourier transform infrared (FTIR) spectroscopy, photoluminescence (PL) emission spectra, UV-vis spectroscopy, and zeta potential (ZP) analysis. The cellular uptake of Suc CDs in the RENCA cell line was investigated by epifluorescence microscopy. The anticancer effect of Suc CDs + DOX under *in vitro* conditions was assessed by standard WST assay. The *in vivo* study of antitumour properties of Suc CDs + DOX was carried out on Balb/c mice and the toxicity of Suc CDs was investigated by the histological analysis.

Materials and methods

Materials

Sucrose, L-serine, quinine sulphate, and dimethyl sulfoxide (DMSO) were purchased from Sigma-Aldrich (NSW, Australia). Amicon® Ultra-Centrifugal Filter Units were purchased from Merck Millipore, Australia. Doxorubicin and adriamycin/doxorubicin HCl were obtained from Pfizer, Australia. The Renca cell lines derived from tumours of BALB/C mice were purchased from ATCC. Dulbecco's phosphate buffered saline (DPBS), Dulbecco's Modified Eagle's Medium (DMEM), fetal bovine serum (FBS), Roswell Park Memorial Institute (RPMI) 1640 media, and trypsin–ethylenediaminetetraacetic acid (EDTA) were purchased from Lonza, Australia. Advanced DMEM/F12 was purchased from Gibco, Australia. NUN Lab-Tek II chamber slide 4 well were purchased from Thermo Fisher Scientific Australia Pty Ltd. A WST-1 Cell Proliferation Assay Kit was purchased from ABCAM Australia. Male Balb/c mice 6–8 weeks old were acquired from Australian Bioresources (ABR).

Methods

Synthesis of sucrose CDs

1.7 g of sucrose and 0.6 g of L-serine were dissolved in 30 ml of ultrapure water in a 50 ml Teflon lined stainless steel hydrothermal autoclave reactor vessel. The vessel was sealed well and placed in an oven heated at 200 °C for 4 h to conduct one pot synthesis of sucrose CDs. After the vessel was cooled to room temperature, the resulting solution was poured into a 50 ml centrifuge tube and centrifuged at 12 000 rpm for 30 min. The supernatant was collected and filtered with a syringe filter (0.22 μm) to remove unreacted residues. Finally, the solution was filtered with an Ultra Centrifugal Filter Unit (MWCO 10 kDa) at 5000*g* for 30 min. The filtrate was collected and the filtration was repeated two more times. Additional separation was carried out using an Ultra Centrifugal Filter Unit (MWCO 3 kDa) at 5000*g* for 30 min. The residue was collected after particles smaller than 2 nm were removed. The pH value of the stock was neutralized using NaOH, and it was stored for further analysis after filtration again with a 0.22 μm syringe filter to get rid of any salt formation during neutralization. The stock solution was stored at 4 °C for further analysis and use. The particles were ultra-sonicated before each assay.

Characterization of sucrose CDs

Transmission electron microscopy imaging was conducted using a TEM (FEI Tecnai 20 TWIN 200 kV) to investigate the size, shape, and size distribution of the as-obtained CDs. The TEM sample was prepared by drop casting the diluted carbon dot suspension on a carbon-film coated copper grid (400 mesh). A Cary 300 Bio UV/vis spectrophotometer was used to record the UV/vis absorption spectrum of the CDs. Fluorescence spectra of the CDs were obtained with a variety of excitation wavelengths using a CLARIOstar spectrometer. The fluorescence quantum yield (QY) of the synthesized CDs was measured by a standard established procedure. Quantum yield was calculated with respect to quinine sulphate (QS) in 0.1 M H_2SO_4 using the formula below:

$$Q_S = Q_R \times \frac{I_S}{I_R} \times \frac{A_R}{A_S} \times \frac{{\eta_S}^2}{{\eta_R}^2}$$

where Q_S = quantum yield of the sample; Q_R = quantum yield of the reference; I_S = area under the PL curve of the sample; I_R = area under the PL curve of the reference; A_R = absorbance of the reference; A_S = absorbance of the sample; η_S = refractive index of the sample; η_R = refractive index of the reference. QY of quinine sulphate = 0.54; refractive index of water = 1.33.

The surface charge of the CDs was measured using a Malvern Zetasizer Nano Series (Nano-ZS). XPS analysis of the CDs drop-cast on Cu tape was carried out using a Thermo Fisher Scientific K-Alpha+ XPS with an Al Kα micro-focused monochromator (1486.68 eV). A Bruker Alpha FTIR was used for functional group analysis.

Drug loading of DOX to sucrose CDs

An identical volume and concentration of DOX and CD solutions in dH_2O were mixed by using a centrifuge and incubated overnight in the dark at 4 °C. The unbound drug was removed by using 3 kDa (MWCO) dialysis tubing for 24 h against dH_2O. The obtained residue in the tube was the drug bound CDs. There was successful drug loading of the Suc CDs with DOX due to electrostatic interaction as sucrose CDs are negatively charged and DOX is positively charged. The drug-loaded CDs were then dried using a freeze-drying machine (Vacuum Freeze Dryer Bk-Fd10s). The UV-vis absorbance spectra of the CDs, unbound drug and drug-loaded CDs were recorded using UV-vis spectroscopy (Cary 300 Bio UV/vis spectrophotometer). The intensity of the DOX characteristic absorbance at 480 nm depended on the concentration of DOX. Therefore, a calibration curve of the absorbance against the concentration of pure DOX solution was generated and used for the loading efficiency of CDs. The loading of the drug was calculated using the following equation.

$$\text{Drug loading}\% = \{\text{concentration of the drug in the conjugate/concentration of drug in feed}\} \times 100\%.$$

The diluted conjugate solution was then read at 480 nm using a UV spectrophotometer, and according to the absorbances obtained from UV-vis spectroscopy in conjunction with the equation $y = mx$, the value of m was calculated to be 0.044 and r^2 of the calibration curve was calculated to be 0.99 (Fig. 1).

Cellular uptake of sucrose CDs

RENCA cells were seeded into a four-chamber slide at a density of 1×10^5 cells per well and incubated for 24 h. The culture medium was removed and washed twice with PBS and fixed with 4% paraformaldehyde, followed by addition of DAPI for cell nucleus staining. Each well was then replaced with 500 μl of medium containing Suc CDs at a concentration of 100 μg ml^{-1} and treated for 2 h at 37 °C. Fluorescence imaging of cells was performed using epifluorescence microscopy (Leica DMI8 Inverted Fluorescent Microscope).

Cell viability and antitumour effect *in vitro*

RENCA cells were seeded with the RPMI-1640 medium, and HK2 cells were seeded in the Advanced DMEM/F12 medium

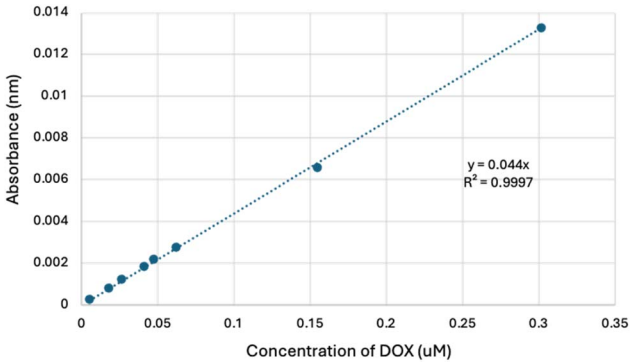

Fig. 1 Calibration curve for doxorubicin.

with 10% FBS and grown at 5% CO_2, in a 37 °C incubator until both cell lines reached a confluency of 80–90%. After that each cell line was seeded into 96 well plates containing 200 μL of medium in each well with 10^4 cells per well. The plates were incubated for 24 h or longer depending on the confluency until they have reached a confluency of 70–80% before the treatment with CDs. The viability was assessed by WST Assay according to the protocol. The WST assay method is based on the cleavage of the tetrazolium salt WST-1 to formazan by mitochondrial dehydrogenases. An increase in the number of viable cells leads to an increase in the activity of mitochondrial dehydrogenases, which in turn results in an increase in the amount of formazan dye produced. The formazan dye produced from WST-1 by viable cells can be quantified by measuring the absorbance of the dye at OD = 440 nm. It is more sensitive than MTT, XTT or MTS-based assays. The absorbance was measured using a SpectraMax iD5 plate reader (BIOSTRATEGY PTY Ltd). The viability was calculated using the following equation: % viability = {OD(sample)/OD (control)} × 100%. All viability graphs were plotted using GraphPad Prism Version8.0a software (GraphPad Software, USA).

Orthotopic tumour cell implantation

Male Balb/c mice 6–8 weeks old were acquired from Australian Bioresources (ABR). The weight of each mouse was approximately 25 g at the beginning of the experiment. All mice experiments were performed under institutional guidelines and regulations and under an approved protocol by the Western Sydney Local Health District Animal Ethics Committee. Surgery was performed under all aseptic conditions Briefly, mice were anesthetized using 2–3% isoflurane. 10 μl cell suspension containing 2×10^5 cells was used. Orthotopic cell implantation to develop a RCC metastatic tumour model in mice and the organ harvest have been carried out according to the protocol.[21]

In vivo antitumour therapeutic efficacy of DOX and Suc CDs + DOX

After 5 days of tumour injection and model development, the treatment was started. The tumour bearing mice were randomly divided into 3 groups including one control group (each group contained 6 mice) and were intravenously injected with pure

DOX and DOX-loaded Suc CDs (Suc CDs + DOX) both at a dose of 4 mg kg^{-1} of body weight *via* the tail vein injection. Mice were dosed once every week for 3 weeks. The body weight was monitored throughout. The mice were sacrificed on the 26th day of the tumour induction, and the tumours were collected to measure the tumour weight. Right and left kidney and lung dissected tissues were harvested and stored in 10% neutralized buffer formalin for 24 h at room temperature. Tissue cassettes were immersed in 70% ethanol for 24 h or longer and further processing of paraffin embedded blocks was done. These tissues were used for immunohistochemistry staining of mice treated with DOX and a Suc CDs + DOX conjugate and the control group for Ki-67 staining.

Conjugation of IR-780 dye to sucrose CDs

The excitation emission window of the sucrose CDs was further increased for the biodistribution study and imaging to avoid autofluorescence from tissues. 2 ml solution of IR-780 dye with a concentration of 10 mg ml^{-1} in methanol was mixed with a 2 ml suspension of Suc CDs with a concentration of 2 mg ml^{-1}. The mixed solution was centrifuged for 5 min and then was left undisturbed overnight at room temperature and further dialysed for 24 h against methanol. Serial dilution of the dye was performed to obtain the absorbance reading using a UV-vis spectrophotometer at 780 nm to find the concentration of the solution using the formula of the standard curve considering the dilution factor. To confirm conjugation of the IR-780 dye to the Suc CDs by electrostatic interaction, zeta potential was tested. The conjugate and IR-780 both should be checked to find if the zeta potential has been changed from that of the original solution.

Biodistribution of the IR-780 and Suc CDs + IR-780 conjugate in a RCC tumour mice model

Post injection of IR-780 and Suc CDs + IR-780 *via* the tail vein using a concentration of 0.25 mg ml^{-1}, both solutions in PBS were imaged using an IVIS Lumina X5 optical imaging System (PerkinElmer) for quantitative *in vivo* and *ex vivo* imaging. The excitation wavelength was 740 nm and emission wavelength was 790 nm. Images were taken at 2, 6, 24, and 48 h and 7 days post injection.

Results and discussion

Characterization of sucrose CDs

The morphology and particle size of the prepared Suc CDs were analysed using TEM as shown in Fig. 2A, Suc CDs are monodispersed and spherical, with an average diameter of 4 nm (Fig. 2B). As shown in Fig. 2C, the sucrose CD dispersion was light brown in colour under daylight and exhibited strong blue luminescence under UV light of 350 nm wavelength. The as prepared Suc CDs emit strong blue fluorescence with a high quantum yield of 58% using quinine sulphate as a reference. There was no reduction in PL intensity after continuous exposure for several days. The FL spectra of the Suc CDs excited at different excitation wavelengths are shown in Fig. 2C and it can be found that the maximum excitation wavelength was located at 340 nm and emission peaks were within the range of 400–450 nm. Fig. 2D displays the UV-vis absorbance spectrum of the prepared Suc CDs in aqueous solution. Two peaks can be observed in the graph at 255 nm and 340 nm. The peak at 255 nm is attributed to the $\pi \rightarrow \pi^*$ transition of C=C present in Suc CDs. To obtain structural understanding and to identify the functional groups on the surface of the prepared Suc CDs, FTIR spectroscopy was used (Fig. 2E). Small peaks in the 890 cm^{-1} and 2900 cm^{-1} region correspond to C–H stretching. The peak at 3272 cm^{-1} corresponds to the strong hydroxyl O–H group and amine (N–H) group. The small peak between 1740 and 1720 cm^{-1} refers to strong C=O stretching. The band at 1509 cm^{-1} corresponds to the strong N–O stretching. The peak between 1380 cm^{-1} and 1370 cm^{-1} refers to medium C–H bending and peak intensity at 1360 cm^{-1} corresponds to C–O– stretching. The band at 976 cm^{-1} refers to strong C=C bonding. Bands between 1305 cm^{-1} and 1200 cm^{-1} might refer to a combination of C–N stretching and N–H bending.[22,23] The FTIR data show the presence of abundant oxygen-containing functionalities and nitrogen containing functional group on the surface of Suc CDs which makes them highly soluble in water and organic solvents.[24,25] Elemental composition characterized by XPS has shown the presence of carbon (C), oxygen (O), nitrogen (N) and hydrogen (H) in the Suc CDs along with some Na (NaOH used for pH adjustments after synthesis). The XPS survey spectrum was used to determine the approximate atomic percentage for each element and the result is shown in Table S1 and Fig. S1 (ESI† data). The atomic percentage for all elements present was calculated using the 1s PE peak. Typically, carbon dots prepared from deionized water yield negatively charged particles with high water solubility. Using different aqueous media like ethanol and other organic solvents leads to hydrophobicity of the carbon dots.[26] The zeta potential of the prepared Suc CDs was measured to be negative, -14 ± 1 mV, at neutral pH and different dilutions (Fig. 2F). Negatively charged particles are less likely to be taken up by macrophages.[27] Sucrose CDs, a novel nanoparticle synthesized for the first time *via* a simple hydrothermal reaction compared to other synthesis processes shown in a previous study where a more complex method of synthesis was used using sucrose, concentrated sulfuric acid and *ortho*-phosphoric acid,[28] demonstrated advantages such as small size for renal clearable, fluorescence, high quantum yield, photostability, high drug loading, non-toxicity, and water solubility. Sucrose has been chosen as the precursor along with L-serine which produced biocompatible carbon dots compared to other studies that shows that fructose or glucose CDs could be toxic at even low concentration.[29] In addition, the CDs showed different emission colours including blue, green and red. The quantum yield of the CDs synthesized from glucose and fructose was reported to be only 1.8%, and 0.3% (ref. 29) respectively, whereas the sucrose CDs have a quantum yield of 58%. The size of the glucose and fructose CDs was also presented to be higher compared to our sucrose CDs.[29] The study assessed the characteristics of sucrose CDs, highlighting the potential of sucrose CDs for further studies.

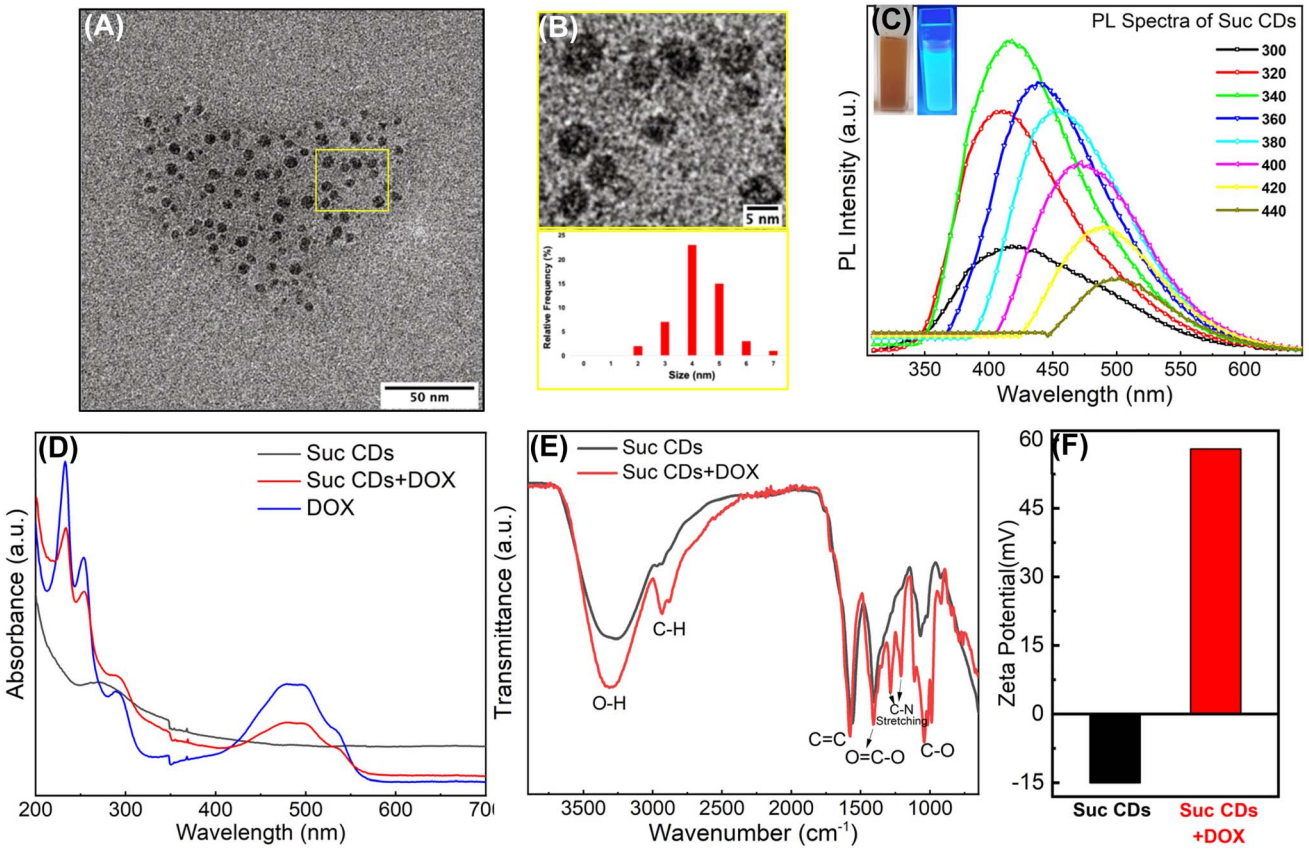

Fig. 2 (A) TEM image of sucrose carbon dot nanoparticles; (B) zoomed-in image of the area (labelled in yellow) of the TEM image of sucrose carbon dots and the particle size distribution; (C) photoluminescence spectrum with absorption and emission spectra of sucrose CDs (inset: aqueous solution of sucrose carbon dots under daylight (left and under UV lamp(right)); (D) UV-vis absorption of Suc CDs, DOX + Suc CDs and DOX in aqueous solution; (E) FTIR spectrum of as prepared sucrose CDs and the Suc CDs + DOX complex; (F) zeta potential change of Suc CDs and the Suc CDs + DOX conjugate.

Drug loading of DOX to Suc CDs

The Suc CDs and DOX form a complex *via* electrostatic interactions or by hydrogen bonds between the carboxylic group on CDs and the amine moiety on DOX.[17,30] The Suc CDs + Dox complex was investigated by UV-vis spectroscopy to confirm successful loading as shown in Fig. 2D.

The Suc CD spectrum (black line) displayed an absorption peak at 350 nm and there was no absorption at around 420 nm to 550 nm, whereas the Dox spectrum (blue line) shows a strong peak at 480 nm. The absorption spectrum of the Suc CDs + Dox complex shows both peaks at around 350 nm and 480 nm (red line), indicating successful conjugation of DOX to sucrose CDs. The loading of DOX to Suc CDs was quantified using UV-vis spectroscopy by measuring the absorbance of the conjugate at 480 nm and calculated to be 50% in deionized water. Batches of conjugation vary by ±2%. Zeta potential of Suc CDs was −14 ± 1 mV and after loading the DOX to Suc CDs the zeta potential increased to +58 mV indicating the successful conjugation of the Suc CDs + Dox as shown in Fig. 2F. Fig. 2E shows FTIR spectra of Suc CDs and the Suc CDs + Dox complex displaying additional and stronger peaks between 1200 cm^{-1} and 900 cm^{-1} referring to a combination of C–N and N–H bonding. There was successful drug loading of the Suc CDs with DOX due to electrostatic bonding between positively charge DOX and negatively charged Suc CDs. The conjugation with DOX has been proved with UV-vis absorption and FTIR data which show the conjugation.

Cellular uptake of carbon dots, cell viability and the *in vitro* antitumour effect

Rapid internalization by cells is an important property for drug delivery. The internalization of Suc CDs was observed by epi-fluorescence microscopy and the results are shown in Fig. 3A. After 2 h incubation with 100 μg ml^{-1} concentration of Suc CDs at 37 °C, it was found that the Suc CDs crossed the cell cytoplasm in Renca and HK2 cell lines suggesting that the CDs can permeate through the cell membrane. Blue fluorescence is observed in the nucleus of the cells due to DAPi staining. The excitation dependent emission of the Suc CDs shows green emission observed under blue illumination. The Suc CDs were not modified with any targeting molecules or chemicals and yet they were successfully taken up into the cells which might be attributed to the surface charge zeta potential and smaller size of the Suc CDs and their specificity for cancer cells as explained

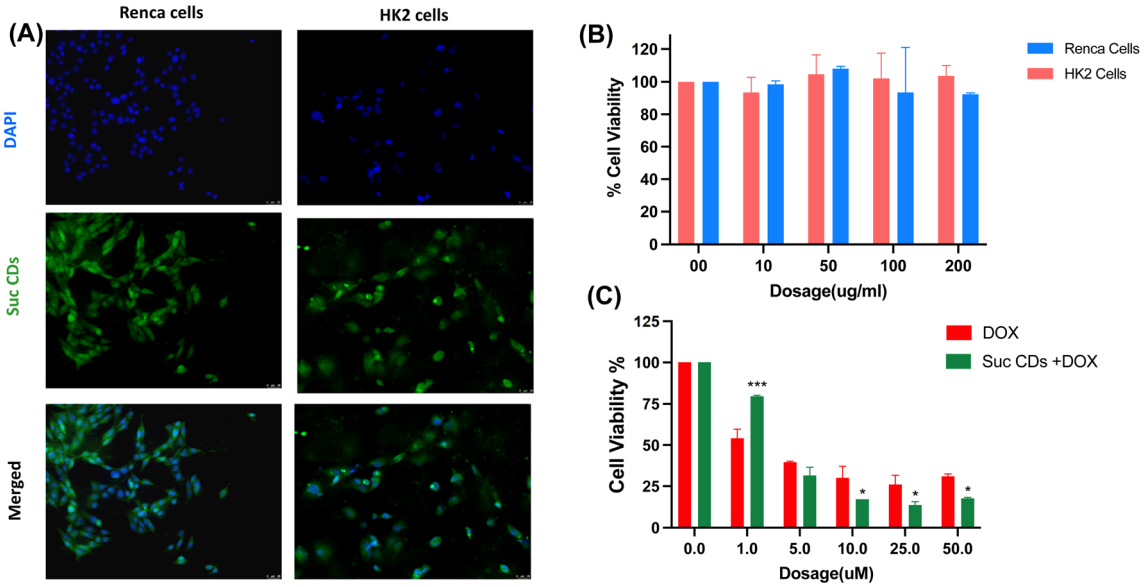

Fig. 3 (A) Endocytosis of Suc CDs observed under epifluorescence microscopy of Renca and HK2 cell lines after incubation with Suc CDs for 2 h. The blue fluorescence is due to DAPI, the carbon dots exhibited green fluorescence, and an overlay image of Renca cells and HK2 cells. The scale bars are 25 μm in all the images; (B) cell viability of HK2 cells (healthy) and Renca cells (cancer) treated with various concentrations of Suc CDs for 48 h with WST-1. The control sample at 0 μg ml^{-1} is the untreated cells; (C) cell viability measured using the WST-1 assay of doxorubicin as a single therapy and in combination with Suc CDs after 48 h incubation in the Renca cell line ($n = 3$, ±SD). The concentration is for DOX alone and the DOX concentration in the conjugates. * Denotes a significant decrease in cell viability compared to single drug treatment ($p < 0.05$).

by the EPR effect. Compared to traditional methods for doxorubicin delivery for solid tumour treatment, the advantage of using carbon nanoparticles include high permeability and retention, high cell internalization, and low cytotoxic to healthy cells and surrounding tissues. Previous studies demonstrated that the DOX + CDs conjugate complex selectively accumulates at the tumour site to induce apoptosis in A549 cells (human lung carcinoma cells). This also demonstrated the targeted delivery of the DOX + CDs conjugate at the tumour site to stimulate apoptosis of A549 cells, thus reducing the effect of free DOX induced necrosis. In addition, they showed that the DOX + CDs group shows higher ability to inhibit tumour growth in comparison to the free DOX group.[31] The uptake of CDs could be through caveolae and clathrin-mediated endocytosis as well as passive diffusion reported by a previous study.[32]

For evaluating the cytotoxicity of the Suc CDs, we selected the renal carcinoma cell line (Renca) and HK2 proximal tubular cell line derived from a normal kidney for comparison. The sucrose CDs possess very low to no toxicity in cells. Suc CDs demonstrate over 90% cell viability at concentrations up to 200 μg ml^{-1} after 48 h, indicating excellent biocompatibility for medical applications (Fig. 3B). In evaluating the impact of DOX and the Suc CDs + DOX complex on Renca cells, WST-1 assay revealed higher cell viability with Suc CDs + DOX at 1 μM compared to DOX alone. IC_{50} for both compounds was achieved at 1 μM and 5 μM concentrations. Notably, Suc CDs + DOX demonstrated reduced cell viability at higher concentrations (5 μM, 10 μM, 25 μM, and 50 μM) compared to DOX alone as shown in Fig. 3C.

In vivo biodistribution and antitumour therapeutic efficacy

Fluorescence imaging using an NIR *in vivo* IVIS system was used to assess signal intensity and biodistribution of IR-780 and Suc CDs + IR-780 in a RCC tumour mice model. Tail vein injection revealed prolonged accumulation of Suc CDs at the tumour site over 24 h and 7 days, emphasizing targeted tumour delivery (Fig. 4A and B). To validate fluorescent properties of Suc CDs conjugated to IR-780 for live animal imaging and localization of the sucrose CD nanoparticles in the tumour site, IR-780 and Suc CDs + IR-780 were injected into the tumour bearing left kidney of the orthotopic RCC mice model. The *in vivo* imaging clearly shows the selective accumulation of Suc CDs + IR-780 at the tumour site which induces NIR fluorescence signalling. The conjugate of Suc CDs + IR-780 is visibly shown to be accumulated at the tumour site for a longer period until 7 days. This is further confirmed with an X-ray image of the mice at 48 h post injection where an overlay image of NIR fluorescence signalling and X-ray image shows signal accumulation at the tumour site and not in other parts of the body (Fig. 4C1 and C2). Therefore, the conjugate allows tumour monitorization by NIR fluorescence imaging and shows the targeted selective accumulation of Suc CDs at the tumour site over a long period of time. *Ex vivo* organ imaging shows the distribution of Suc CDs + IR-780 in the internal organs. At 24 h p.i, the signal is mostly in the lung, liver, and both kidneys. After 7 days post injection there is a signal only in the tumour bearing left kidney which shows accumulation of the conjugate at the tumour site (Fig. 4D). A comparison graph (Fig. 4E) highlights the significant accumulation of Suc CDs + IR-780 in the tumour-bearing kidney until 7 days, while bare IR-780 is rapidly cleared from the body (Fig. 4F).

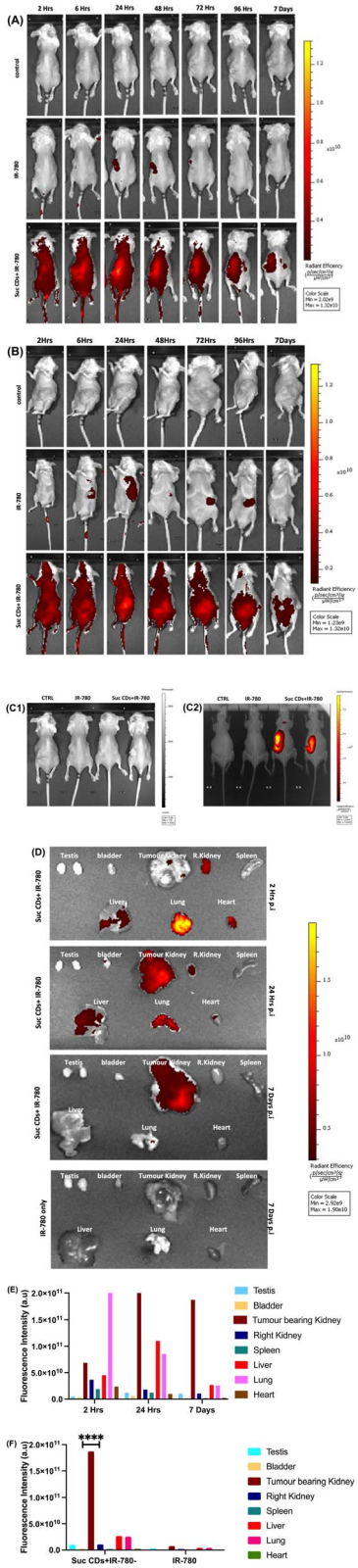

Fig. 4 (A and B) The *in vivo* biodistribution of IR-780 and Suc CDs + IR-780 at different time points (2, 6, 24, 48, 72, and 96 h, and 7 days) after i.v. injection in the RCC tumour model (dorsal position-A and supine position-B) at an excitation wavelength of 740 nm and emission wavelength of 790 nm; (C) 48 h post i.v injection of IR-780 and Suc CDs + IR-780 in tumour bearing mice showing the normal brightfield image (C1) and overlay NIR fluorescence and X-ray imaging (C2) showing localization of Suc CDs + IR-780 at the tumour site (left kidney). (D) *Ex vivo* NIR fluorescence images of the organs isolated from Suc CDs + IR-780 and Ir-780 only injected tumour bearing mice at 2 h, 24 h and 7 days post injection; (E) NIR fluorescence intensity of the signal in the isolated organs of the Suc CDs + IR-780 mice over a period of 2 h, 24 h and 7 days post injection in RCC tumour bearing mice; and (F) NIR fluorescence intensity of the signal from Suc CDs + IR-780 and IR-780 alone in 7 days post injection RCC tumour bearing mice.

In an RCC tumour mice model, DOX and CDs + DOX were injected weekly for 3 weeks at a dose of 4 mg kg^{-1} of body weight, resulting in an 88% decrease in tumour weight for DOX alone and a remarkable 96% decrease for Suc CDs + DOX compared to the control group. The conjugate showed an additional 8% reduction in tumour growth compared to free DOX, with no significant side effects observed (Fig. 5A and B). The tumour growth inhibition rates for the free DOX and Suc CDs + DOX group were calculated to be 89% and 96%, respectively. IHC analysis explored Ki-67 expression in tumours. The control group exhibited the highest Ki-67 expression in the tumour-bearing kidney and lungs. DOX and Suc CDs + DOX groups showed reduced Ki-67 expression, correlating with decreased tumour weight. Suc CDs + DOX demonstrated lower Ki-67 expression than DOX alone in tumour-bearing kidney sections. The software quantified positive Ki-67 cells, revealing increased expression in control group kidneys and lungs due to metastasis. Suc CDs + DOX exhibited a significant decrease in Ki-67 expression in the left kidney compared to DOX alone. No significant decrease in Ki-67 expression was observed in lungs for both treatment groups, indicating better survival (Fig. 5C and D).

Lung metastasis can be detected by 15 days after tumour implantation and was present in almost all animals by day 21. No liver metastasis was observed in our study which was found in another study.[33] The software quantified positive Ki-67 cells, revealing increased expression in control group kidneys and lungs due to metastasis. Suc CDs + DOX exhibited a significant decrease in Ki-67 expression in the left kidney compared to DOX alone. No significant decrease in Ki-67 expression was observed in lungs for both treatment groups, indicating better survival (Fig. 5C and D).[34]

In vivo side effect assessment

The cortical tubule cell height decreased in the DOX-treated group's contralateral kidney, suggesting cellular atrophy. In contrast, Suc CDs + DOX treated mice showed a significantly lower decrease, indicating potentially lower injury compared to that of DOX treated mice in normal renal tubular cells as shown in Fig. 5E. The higher inhibition of tumour weight in Suc CDs + DOX might be explained by targeted delivery of Suc CDs + DOX and efficient accumulation at tumour sites *via* the EPR effect.[32] Due to selective delivery and release and localization of the Suc CDs (found *via in vivo* imaging of Suc CDs + IR-780), the conjugate of Suc CDs + DOX does not show any adverse effect, and thus Suc CDs can be used as a promising nanocarrier for the transportation of DOX and reducing systemic toxicity.

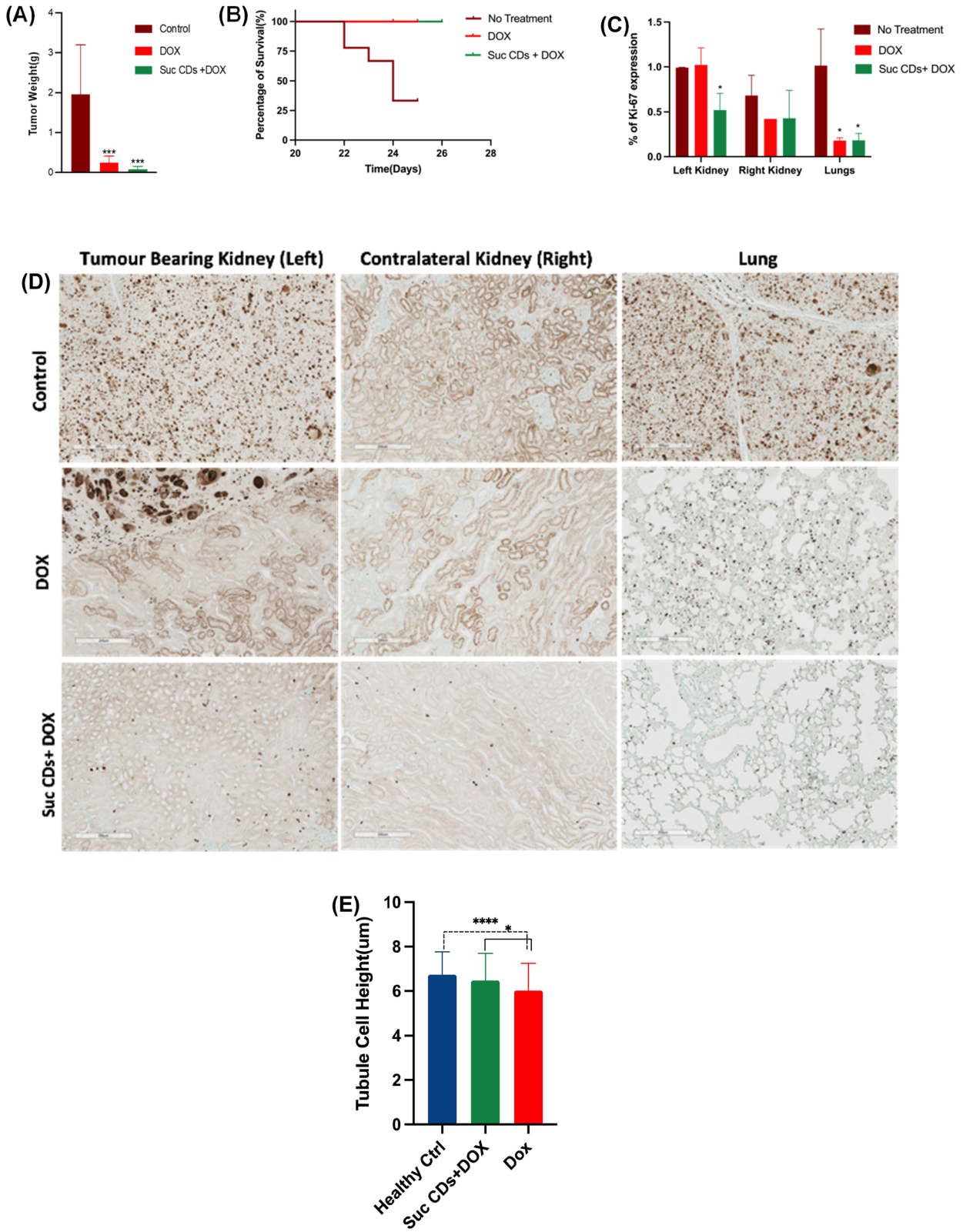

Fig. 5 (A) Tumour growth inhibition by DOX and Suc CDs + DOX in a Balb/c tumour bearing RCC mice model after tail-vein injection of DOX and Suc CDs + DOX ($n = 6$, dose: 4 mg kg^{-1} mouse body weight). Tumour weight (g) in no treatment (control), and tumour weight reduction in free DOX, and Suc CDs + DOX treatments; (B) survival proportion in mice in no treatment *vs.* treatment groups (DOX and Suc CDs + DOX) over 26 days; (C) percentage of tumour cells represented in parallel to expression of KI-67 in the tissue sections of the mice with Aperio Imagescope software; (D) *ex vivo* IHC analysis of expression of ki-67 with a methyl green counterstain in tissue sections from the tumour bearing kidney (Left), contralateral kidney (Right) and the lung in the control, DOX alone and Suc CDs + DOX group at 10× (scale bar = 200 μm); (E) mean cross-sectional normal renal tubule cell height in the contralateral kidney (non-tumour kidney) for healthy control, Suc CDs + DOX and DOX alone treatment groups. (**P value = 0.023, $P < 0.05$).

Conclusion

We have successfully developed cost-effective novel nanoparticles called sucrose carbon dots with a size less than 5 nm possessing renal clearable properties with a high fluorescence quantum yield. They are soluble both in water and organic solvents with good photostability and chemical stability and do not form any precipitate over time. These Suc CDs are biocompatible with no effect on cell viability and no effect on healthy mice models. The renal clearable sucrose CDs can be used as a carrier of anticancer agents such as DOX for effective treatment in tumour bearing mice. The synthesized Suc CDs conjugated to DOX effectively inhibit growth in the Renca cell line. The tumour bearing Balb/c mice showed additional tumour growth suppression in Suc CDs + DOX mice compared to DOX alone. The Suc CDs + DOX group has less toxicity to normal tubule cells. The off-target side effects of DOX can be reduced by passive targeting of sucrose CDs due to the EPR effect. The accumulation of Suc CDs is observed at the tumour site for a longer time in tumour bearing mice confirming fluorescent properties of Suc CDs conjugated to IR-780 for live animal imaging and localization of the sucrose CD nanoparticles. Hence, the sucrose CDs can be used for imaging in live animals and used as a biocompatible florescent nanocarrier to carry cancer drugs specifically to the tumour site without any cancer-targeting moiety to reduce off site targeting. Suc CDs conjugated to DOX can avoid non-targeted delivery of DOX to healthy tissues in the body and these renal clearable sucrose CDs can be used as a nanocarrier for the transportation of DOX and reducing systemic toxicity of DOX and other anticancer agents for effective treatment of cancer and potential clinical uses in the future.

Data availability

(1) Publicly available data: the data supporting the findings of this study are publicly available as part of the author's (Farhana Azmi) thesis in the University of Sydney's institutional repository at **https://ses.library.usyd.edu.au/handle/2123/31189**. (2) Data included as the ESI:† some of the data supporting the findings of this study are included in the ESI† accompanying this article.

Author contributions

FA, XX, QC and YW conceived of the presented idea, and designed and supervised the study. FA, QC and YW performed animal experiments and *in vitro* experiments. FA, XX, QC and YW analysed the data, participated in discussions, provided intellectual input and wrote the manuscript. All authors contributed to the article and approved the submitted version.

Conflicts of interest

There are no conflicts to declare.

Acknowledgements

We are grateful to the Penfold family for providing 'The Stephen and Barbara Penfold PhD scholarship' to the PhD student. This work was also supported by the National Health & Medical Research Council of Australia (NHMRC, grants 2008347 and 2012351). Library preparation was performed at the Westmead Scientific Platforms, which are supported by the Westmead Institute for Medical Research, the Cancer Institute New South Wales and the National Health and Medical Research Council. We thank Maggie Wang, Hui Zhang, Hong Yu, Li Ma, Laurence Cantrill and Emma kettle from Westmead Core Facilities for technical assistance. Special acknowledgement to Hui Zhang and Emma Kettle for their additional assistance with the *in vivo* and TEM imaging. We express gratitude to Dr Paul Fitzgerald, Dr Joonsup Lee, Dr Michelle Wood and other members from the Vibrational Spectroscopy team and Key Centre for Polymers and Colloids from The University of Sydney.

References

1 L. Cirillo, S. Innocenti and F. Becherucci, Global Epidemiology of Kidney Cancer, *Nephrol., Dial., Transplant.*, 2024, **39**(6), 920–928, DOI: **10.1093/ndt/gfae036**.
2 I. Hamaidi, C. Coquard, S. Danilin, V. Dormoy, C. Béraud and S. Rothhut, The Lim1 oncogene as a new therapeutic target for metastatic human renal cell carcinoma., *Oncogene*, 2019, **38**(1), 60–72, DOI: **10.1038/s41388-018-0413-y**.
3 W. Linehan and C. Ricketts, RCC-advances in targeted therapeutics and genomics, *Nat. Rev. Urol.*, 2016, **14**(2), 76–78, DOI: **10.1038/nrurol.2016.260**.
4 J. Hsieh, M. Purdue, S. Signoretti, C. Swanton, L. Albiges, M. Schmidinger, *et al.*). Renal cell carcinoma, *Nat. Rev. Dis. Primers*, 2017, **3**, 17009, DOI: **10.1038/nrdp.2017.9221**.
5 R. L. Siegel, S. A. Fedewa, K. D. Miller, A. Goding-Sauer, P. S. Pinheiro, D. Martinez-Tyson and A. Jemal, Cancer statistics for Hispanics/Latinos, 2015, *Ca-Cancer J. Clin.*, 2015 Nov-Dec, **65**(6), 457–480.
6 T. Choueiri and R. Motzer, Systemic Therapy for Metastatic Renal-Cell Carcinoma, *N. Engl. J. Med.*, 2017, **376**(4), 354–366, DOI: **10.1056/nejmra1601333**.
7 H. Koul, J. S. Huh, K. O. Rove, L. Crompton, S. Koul, R. B. Meacham and F. J. Kim, Molecular aspects of renal cell carcinoma: a review, *Am. J. Cancer Res.*, 2011, **1**(2), 240–254.
8 A. Rodriguez-Vida, T. Hutson, J. Bellmunt and M. Strijbos, New treatment options for metastatic renal cell carcinoma, *ESMO Open*, 2017, **2**(2), e000185, DOI: **10.1136/esmoopen-2017-000185**.
9 R. Misra, S. Acharya and S. Sahoo, Cancer nanotechnology: application of nanotechnology in cancer therapy, *Drug Discovery Today*, 2010, **15**(19–20), 842–850, DOI: **10.1016/j.drudis.2010.08.006**.
10 H. Lu and M. Stenzel, Multicellular Tumour Spheroids (MCTS) as a 3D *In Vitro* Evaluation Tool of Nanoparticles, *Small*, 2018, **14**(13), 1702858, DOI: **10.1002/smll.201702858**.

11 S. Lim, W. Shen and Z. Gao, Carbon quantum dots and their applications, *Chem. Soc. Rev.*, 2015, **44**(1), 362–381, DOI: 10.1039/c4cs00269e.
12 R. Williams, E. Jaimes and D. Heller, Nanomedicines for kidney diseases, *Kidney Int.*, 2016, **90**(4), 740–745, DOI: 10.1016/j.kint.2016.03.041.
13 J. Liu, M. Yu, C. Zhou, *et al.*, Renal clearable inorganic nanoparticles: a new frontier of bionanotechnology, *Mater. Today*, 2013, **16**, 477–486.
14 G. Nocito, G. Calabrese, S. Forte, S. Petralia, C. Puglisi, M. Campolo, *et al.*). Carbon Dots as Promising Tools for Cancer Diagnosis and Therapy, *Cancers*, 2021, **13**(9), 1991, DOI: 10.3390/cancers13091991.
15 M. Longmire, P. Choyke and H. Kobayashi, Clearance properties of nano-sized particles and molecules as imaging agents: considerations and caveats, *Nanomedicine*, 2008, **3**(5), 703–717, DOI: 10.2217/17435889.3.5.703.
16 N. Dengina, I. Tsimafeyeu and T. Mitin, Current Role of Radiotherapy for Renal-Cell Carcinoma: Review, *Clin. Genitourin. Cancer*, 2017, **15**(2), 183–187.
17 Y. Jung, E. Shin and B. Kim, Cell Nucleus-Targeting Zwitterionic Carbon Dots, *Sci. Rep.*, 2015, **5**(18807), DOI: 10.1038/srep18807.
18 Q. Zeng, D. Shao, X. He, Z. Ren, W. Ji, C. Shan, *et al.*). Carbon dots as a trackable drug delivery carrier for localized cancer therapy *in vivo*, *J. Mater. Chem. B*, 2016, **4**(30), 5119–5126, DOI: 10.1039/c6tb01259k.
19 K. Gayathri and R. Vidya, Carbon nanomaterials as carriers for the anti-cancer drug doxorubicin: A review on theoretical and experimental studies, *Nanoscale Adv.*, 2024, **6**(16), 3992–4014, DOI: 10.1039/d4na00278d.
20 J. Zhang, *et al.*) 'doxorubicin-loaded carbon dots lipid-coated calcium phosphate nanoparticles for visual targeted delivery and therapy of tumor, *Int. J. Nanomed.*, 2020, **15**, 433–444, DOI: 10.2147/ijn.s229154.
21 A. Tracz, M. Mastri, C. Lee, R. Pili and J. Ebos, Modeling Spontaneous Metastatic Renal Cell Carcinoma (mRCC) in Mice Following Nephrectomy, *J. Visualized Exp.*, 2014, (86), 51485, DOI: 10.3791/51485.
22 F. Ashrafi Tafreshi, Z. Fatahi, S. Ghasemi, A. Taherian and N. Esfandiari, Ultrasensitive fluorescent detection of pesticides in real sample by using green carbon dots, *PLoS One*, 2020, **15**(3), e0230646, DOI: 10.1371/journal.pone.0230646.
23 P. Chauhan, J. Saini, S. Chaudhary and K. Bhasin, Sustainable synthesis of carbon dots from agarose waste and prospective application in sensing of l-aspartic acid, *Mater. Res. Bull.*, 2021, **134**, 111113, DOI: 10.1016/j.materresbull.2020.111113.
24 H. Shabbir, E. Csapó and M. Wojnicki, Carbon quantum dots: The role of surface functional groups and proposed mechanisms for metal ion sensing, *Inorganics*, 2023, **11**(6), 262, DOI: 10.3390/inorganics11060262.
25 D. Ozyurt, *et al.*) 'Properties, synthesis, and applications of Carbon Dots: A Review, *Carbon Trends*, 2023, **12**, 100276, DOI: 10.1016/j.cartre.2023.100276.
26 F. Cheng, X. An, C. Zheng and S. Cao, Green synthesis of fluorescent hydrophobic carbon quantum dots and their use for 2,4,6-trinitrophenol detection, *RSC Adv.*, 2015, **5**(113), 93360–93363, DOI: 10.1039/c5ra19029k.
27 S. Wilhelm, A. J. Tavares, Q. Dai, *et al.*, Analysis of nanoparticle delivery to tumours, *Nat. Rev. Mater.*, 2016, **1**, 16014.
28 U. Yunus, *et al.*) 'Targeted drug delivery systems: Synthesis and *in vitro* bioactivity and apoptosis studies of gemcitabine-carbon dot conjugates, *Biomed. Mater.*, 2020, **15**(6), 065004, DOI: 10.1088/1748-605x/ab95e1.
29 S. Cailotto, *et al.*) 'Carbon dots from sugars and ascorbic acid: role of the precursors on morphology, properties, toxicity, and drug uptake, *ACS Med. Chem. Lett.*, 2018, **9**(8), 832–837, DOI: 10.1021/acsmedchemlett.8b00240.
30 Q. Zeng, D. Shao, X. He, Z. Ren, W. Ji, C. Shan, *et al.*). Carbon dots as a trackable drug delivery carrier for localized cancer therapy *in vivo*, *J. Mater. Chem. B*, 2016, **4**(30), 5119–5126, DOI: 10.1039/c6tb01259k.
31 L. Yang, Z. Wang, J. Wang, W. Jiang, X. Jiang, Z. Bai, *et al.*). Doxorubicin conjugated functionalizable carbon dots for nucleus targeted delivery and enhanced therapeutic efficacy, *Nanoscale*, 2016, **8**(12), 6801–6809, DOI: 10.1039/c6nr00247a.
32 S. Zhu, *et al.*) 'Photoluminescent graphene quantum dots for *in vitro* and *in vivo* bioimaging using long wavelength emission, *RSC Adv.*, 2015, **5**(49), 39399–39403, DOI: 10.1039/c5ra02961a.
33 P. Sobczuk, A. Brodziak, M. Khan, S. Chhabra, M. Fiedorowicz, M. Wełniak-Kamińska, K. Synoradzki, E. Bartnik, A. Cudnoch-Jędrzejewska and A. Czarnecka, Choosing The Right Animal Model for Renal Cancer Research, *Transl. Oncol.*, 2020, **13**(3), 100745.
34 Y. Yuan, B. Guo, L. Hao, N. Liu, Y. Lin, W. Guo, *et al.*). Doxorubicin-loaded environmentally friendly carbon dots as a novel drug delivery system for nucleus targeted cancer therapy, *Colloids Surf., B*, 2017, **159**, 349–359, DOI: 10.1016/j.colsurfb.2017.07.030.